Inorganic Chemistry

Article

pubs.acs.org/IC

Self-Assembly of Three-Dimensional $SrTiO_3$ Microscale Superstructures and Their Photonic Effect

Xiaoliang Yuan,[†] Maojun Zheng,*[,†] Yafeng Zhang,[‡] Tao Zhou,[†] Changli Li,[†] Xiaosheng Fang,[§] Li Ma,[†] and Wenzhong Shen[†]

[†]Key Laboratory of Artificial Structures and Quantum Control, Ministry of Education, Department of Physics, Shanghai Jiao Tong University, Shanghai 200240, People's Republic of China

[‡]Department of Physics, Fudan University, Shanghai 200433, People's Republic of China

[§]Department of Materials Science, Fudan University, Shanghai 200433, People's Republic of China

Supporting Information

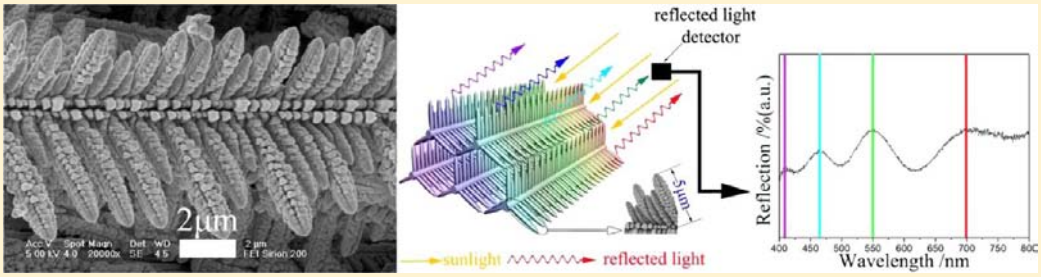

ABSTRACT: 3D $SrTiO_3$ microscale superstructures (STOMSs) have been prepared *via* hydrothermal synthesis and multiple (five times) crystallization process. Branches and trunks on STOMSs show perfect corn-like structures, and each side of the trunks could be considered as grating-analogous structures. These well-ordered trunks along with gratings constitute 3D hybrid microstructures that contribute to light diffraction, and the colorful photonic effects of light diffraction are thought to be due to refractive index modulations in three dimensions. The colors of STOMSs can be tuned from yellow to cyan by changing the growth cycle. This special optical performance could broaden the application scope of $SrTiO_3$.

1. INTRODUCTION

Transition metal oxides with a cubic perovskite structure $ATiO_3$ (A = Ba, Sr, Ca) have been of great interest in science and engineering in the electronics industry and are noteworthy for their advantageous dielectric, ferroelectric, piezoelectric, thermoelectric, superconducting, electrostrictive, and electro-optic properties with corresponding applications.[1−6] Among these materials, strontium titanate ($SrTiO_3$), as an ideal substrate material for epitaxial growth of many functional materials and with its own high dielectric constant, thermal stability, and photocatalytic properties, serves as one of the most versatile functional materials in a wide range of technological uses.[7−11] Generally, $SrTiO_3$ is prepared by solid-state reaction[12,13] of strontium carbonate and titanium dioxide, typically at temperatures higher than 900 °C. $SrTiO_3$ powders obtained from this traditional method are generally microstructural variations due to the lack of control over the physical and chemical characteristics, which always leads to poor property optimization and reproducibility. Although there have been various reports on the synthesis strategies of $SrTiO_3$ particles and films in recent years, such as epitaxial growth by chemical vapor deposition (CVD),[14,15] magnetron sputtering,[16] or sol−gel,[17,18] the precisely controllable synthesis of microscale or even nanoscale morphologic and structural crystalline particles and thin films is less than satisfactory. In contrast to other techniques, the hydrothermal method[19−23] offers an inexpensive and environmentally friendly route and the ability to control chemical composition, homogeneity, purity, morphology, shape, and phase composition of the nanostructure materials under moderate conditions. By the way, this synthesis strategy has greatly accelerated the development of a large number of inorganic[24−28] and organic[29−31] superstructure materials in recent years, which are widely used in many fields such as photonic devices, energy storage, and microvessels for drug delivery, biomedical diagnosis agents, nanoscale reactors, humidity sensors, and catalysts for size-selective reactions. Due to its potential application, the synthesis and study of $SrTiO_3$ superstructure material remains urgent nowadays. Furthermore, although the study on ferroelectric thin film photonic crystals[32,33] has developed for several years, synthesis of 3D structure ferroelectric photonic crystals is still a new topic and a challenge for their future applications.

Here we report new findings on the formation and evolution of pure 3D $SrTiO_3$ microscale superstructures (STOMSs) based on the synthesis strategy of hydrothermal methods, and the mechanism of self-assembly (SA) behavior has been discussed by the multiple crystallization process with the

Received: November 27, 2012
Published: February 12, 2013

 © 2013 American Chemical Society dx.doi.org/10.1021/ic302585g | *Inorg. Chem.* 2013, 52, 2581−2587

rhythmic cooling approach. What is more interesting, each branch on the trunk shows a corn-like structure. On the basis of experimental data, we concluded that the growth of complex microscale superstructures can be explained only *via* progressive assembly and multiple crystallization processes, which are advantageous for the SA of STOMSs compared to long-time (5 days) hydrothermal reactions without rhythmic cooling. Meanwhile, periodical structure leads to a colorful photonic effect, and the colors are obvious and controllable and vary from yellow to cyan. Furthermore, grating-analogous structures clearly exist if we simplify the complicated, interconnected 3D microstructures of trunks and branches, taking into account only one side of the trunk, and various reflected light is thought to originate from diffraction grating effects. This approach is simple and cost-effective in fabricating 3D STOMSs for practical photonic applications.

2. EXPERIMENTAL SECTION

Preparation of TiO_2 Nanotube Films. The template TiO_2 films, which were used for the synthesis of STOMSs, were fabricated *via* two-step anodization under high field in our preparatory work.[34] Polished Ti foils were put into a tailor-made holder with a circular area of 2 cm^2 exposed to the electrolyte (0.3 wt % ammonium fluoride (NH_4F) and 4 vol % water in ethylene glycol (96 vol %)). The TiO_2 films were obtained in 4 h *via* anodization. After 24 h of drying in air, the oxide layers, with a thickness of about 100 μm, were isolated automatically, as shown in Figure S1a, and were used in the next hydrothermal synthesis experiments.

Synthesis of 3D $SrTiO_3$ Superstructures. For the synthesis of $SrTiO_3$, strontium chloride ($SrCl_2$, ≥99.5%), calcium chloride ($CaCl_2$, ≥96%), potassium hydroxide (KOH, ≥90%), and anodic TiO_2 precursor were used. Solutions had the following composition: Sr^{2+} 50−200 mM, Ca^{2+} 50−100 mM, and OH^- 0.2−4.0 M. However, the optimal reaction solutions have been proved to be composed of Sr^{2+} 100 mM, Ca^{2+} 50 and 100 mM, and OH^- 1.0 and 2.0 M. First, $SrCl_2$, $CaCl_2$, and KOH were dissolved in a glass beaker by stirring at room temperature for 1 h. Second, a white precipitate was separated *via* filter operation in order to get clear synthesis solutions. Third, clear synthesis solutions and TiO_2 films were transferred to a Teflon-lined stainless steel autoclave and heated at 160 °C in an oven for 10 h. Then crystallization of $SrTiO_3$ occurred accompanied with a natural cooling process to room temperature. This heating and cooling process should be repeated five times at least. Lastly, washing in a 1% dilute hydrochloric acid bath at 60 °C for 5 h to dissolve the fluffy $Ca(OH)_2$ layers and drying the as-obtained $SrTiO_3$ were necessary.

Characterization of Materials. The morphologies of our $SrTiO_3$ samples were observed using a field-emission scanning electron microscope (FESEM, Philips XL30FEG). Energy dispersive X-ray spectroscopy (EDS, INCA Oxford) was recorded at the surface of the structure. Crystal structures of samples were examined using X-ray diffraction (XRD, Bruker-AXS). The composition of the mother liquors (taken from the autoclave after the synthesis) was determined by inductively coupled plasma atomic emission spectrometry (ICP-AES, THERMO). Optical reflection of colorful and photonic samples was observed by an optical microscope system (Leica). The morphology and electron diffraction of the crystals were examined by transmission electron microscopy (TEM, JEOL), while specimens were prepared by dispersing the purified structures on carbon-foam-coated copper grids. The crystallinity of $SrTiO_3$ was determined using selected area electron diffraction (SAED) coupled with TEM.

3. RESULTS AND DISCUSSION

Ordered TiO_2 nanotube (TiNT) arrays were fabricated *via* two-step anodization under high field based on our previous work,[34] as shown in Figure S1a. Then, *in situ* synthesis of STOMSs *via* the hydrothermal method and multiple (five times) crystallization took place on the surface of these TiNTs. Figure S1b−d shows digital photographs of as-prepared $SrTiO_3$ films. It is clear that variable pH values of the synthesis solutions led to clearly visible and variable colors (cyan and yellow) by the naked eye. Moreover, these variable colors have been proved to be caused by their 3D microstructures.

It is noticed that the 3D skeletons of $SrTiO_3$ were not being broken even if the films had been smashed into pieces during the hydrothermal reaction, which was totally attributed to the perfect supporting effect of the TiNT nanostructure arrays. It has been observed that the tube walls of TiNT act as a growing point and the 3D skeleton of $SrTiO_3$ grows along these TiNTs, as shown in Figure 1 and Figure 2. Hence, TiNT precursors

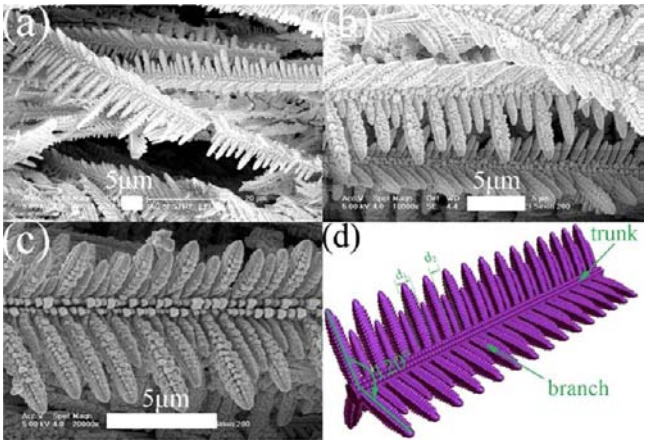

Figure 1. (a−c) Typical SEM images with different azimuths and magnification of 3D STOMSs synthesized at 160 °C in optimal solutions with 100 mM Sr^{2+}, 50 mM Ca^{2+}, and 2 M OH^-. (d) Schematic representation of the single hyperbranched $SrTiO_3$ structural unit.

along with a high concentration of OH^- in the mother liquors act as uniquely convenient mediums for the self-assembly of STOMSs because they provide $[Ti(OH)_6]^{2-}$ slowly and continuously. In order to obtain an optimum OH^- concentration in our reactions, SEM images of STO fabricated in different concentrations of OH^- have been observed, as shown in Figure 3. It is found that the rudiments of STOMSs exist only when the concentration of KOH is 1.0 M in the reaction solutions, and the rudiments will grow into 3D STOMSs if the concentration of KOH is greater than 1.0 M. Hence, the study of the synthesis mechanism is performed based on the optimal 2.0 M KOH solution system. However, if the concentration of KOH is less than 1.0 M, only STO particles could form on the surface of TiO_2, as shown in Figure 3a, b. Hence, a high concentration of KOH is thought to be the dominant factor in synthesizing 3D STOMSs. By the way, if the assembly medium is TiO_2 particles[22] or another titanium salt solution ($TiOCl_2$),[35] the final products should be $SrTiO_3$ particles. Figure 1a−c shows the typical SEM images of the STOMSs synthesized at 160 °C in the optimal solutions with Sr^{2+} 100 mM, Ca^{2+} 50 mM, and OH^- 2 M *via* hydrothermal synthesis and multiple (five times) crystallization. We could see perfect 3D $SrTiO_3$ superstructures with different azimuths and magnification. A schematic representation of the single $SrTiO_3$ superbranched structure unit will help us understand the 3D structure more clearly, as shown in Figure 1d.

To understand the mechanism and the effect of pH, the chemical reactions must be considered. Similar to the typical

dx.doi.org/10.1021/ic302585g | Inorg. Chem. 2013, 52, 2581−2587

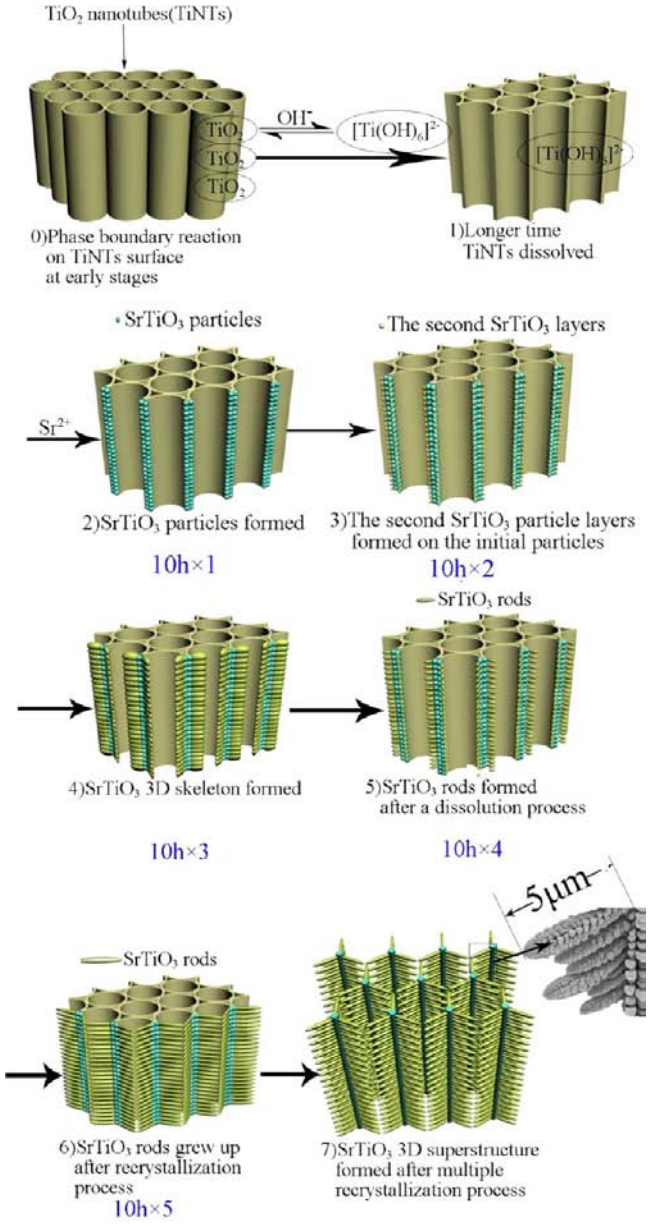

Figure 2. Synthesis mechanism of STOMSs at each step.

transformation from titanium oxide to titanate, the formation of STOMSs also involves a dissolution−precipitation process.[36,37] Figure 2 shows the synthesis mechanism of STOMSs at each step. On the basis of AAO (anodic aluminum oxide)-template-assisted growth of ZnO and other semiconductor materials,[38,39] we adopted this method in our experiment. However, the difference is that AAO did not take part in the hydrothermal synthesis reaction, compared to TiNT layers. TiNT layers not only are used as precursors to provide titanium ions but also act as skeletons and growing points. Hence, the Ti−O bonds on the TiO_2 precursors must be broken *via* hydrolytic attack to form soluble $[Ti(OH)_6]^{2-}$ at the early stage (steps 0 and 1). This process is described below:

$$TiO_2 + 2OH^- + 2H_2O \rightarrow [Ti(OH)_6]^{2-} \quad (1)$$

Determination of the mother liquors *via* ICP-AES (Figure S2 and Table S1) shows that the chemical composition of titanium increases after the first 10 h, which means that there are large

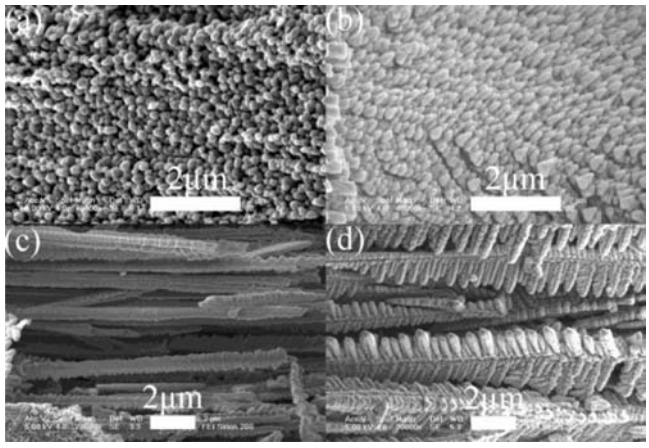

Figure 3. SEM images of STO ($SrTiO_3$) fabricated in different concentrations of OH^-: in a (a) 0.3 M KOH solution, (b) 0.5 M KOH solution, (c) 1.0 M KOH solution, and (d) 1.5 M KOH solution.

amounts of $[Ti(OH)_6]^{2-}$ in the mother liquors due to reaction 1. It is worth noting that the concentration of OH^- should be large enough to ensure the dissolution of TiNT layers during the whole synthesis process. Then, precipitation of $SrTiO_3$ takes place according to the following reaction on the dissolved TiNT skeletons:

$$Sr^{2+} + [Ti(OH)_6]^{2-} \rightarrow SrTiO_3 + 2H_2O \quad (2)$$

The total phase boundary reaction is

$$TiO_2 + Sr(OH)_2 \rightarrow SrTiO_3 + H_2O \quad (3)$$

Dissolution of TiO_2 and precipitation of $SrTiO_3$ occur at the same time in the vicinity of the nanotube surfaces due to a large amount of OH^-, and therefore, contiguous TiNTs are easy to break at the tangency point and $SrTiO_3$ will preferentially and spontaneously nucleate at the cross section. As time progresses, $SrTiO_3$ particle layers (the rudiment of STOMSs) form gradually within the initial crystallization process (sustained for 10 h), which are loosely packed (step 2). To explain the formation of particle layers, the oriented attachment mechanism[40,41] should be considered in the initial crystallization process. In this stage, TiNTs act as skeletons and physical adhesion points, and $SrTiO_3$ particles will attach to the TiNT walls along a tangential orientation to reduce the surface free energy. The driving forces for attachment are thought to be van der Waals and electrostatic interactions. As time goes on, the STOMS rudiments will be formed after precipitating crystallization, which is considered to be the key step for the whole process. These as-formed rudiments will be easy to grow into three-dimensional microstructures after the first crystallization process. Then in step 3, the initial $SrTiO_3$ particle layers stop growing and the second particle layers will start piling up and fusing on the rudiments during another 10 h of hydrothermal and crystallization process. Follow this step, the second particle layers pile up and fuse sequentially until $SrTiO_3$ 3D skeletons have been formed (step 4). Next, $SrTiO_3$ rods form gradually *via* a chemical dissolution−precipitation process by step 5. Similar to that proposed for $BaTiO_3$,[42] a reverse reaction occurs in this stage, which can be described as follows:

$$SrTiO_3 + 2H_2O \rightarrow Sr^{2+} + [Ti(OH)_6]^{2-} \quad (4)$$

A direct proof of reaction 4 is the chemical composition of mother liquors (determined by ICP-AES) after hydrothermal

dx.doi.org/10.1021/ic302585g | Inorg. Chem. 2013, 52, 2581−2587

reaction, as shown in Figure S2 and Table S1. It is noticed that the chemical composition of titanium increases after the fourth 10 h stage, owing to a large amount of reaction products of $[Ti(OH)_6]^{2-}$ by eq 4. This stage is also thought to be important for the formation of $SrTiO_3$ rods. Eventually, $SrTiO_3$ rods grow during the fifth hydrothermal reaction (steps 6 and 7). In particular, all steps should contain 10 h of hydrothermal reaction and 24 h of cooling crystallization process. SEM images observed at each growth stage will help us understand the synthesis mechanism of 3D STOMSs, as shown in Figure 4.

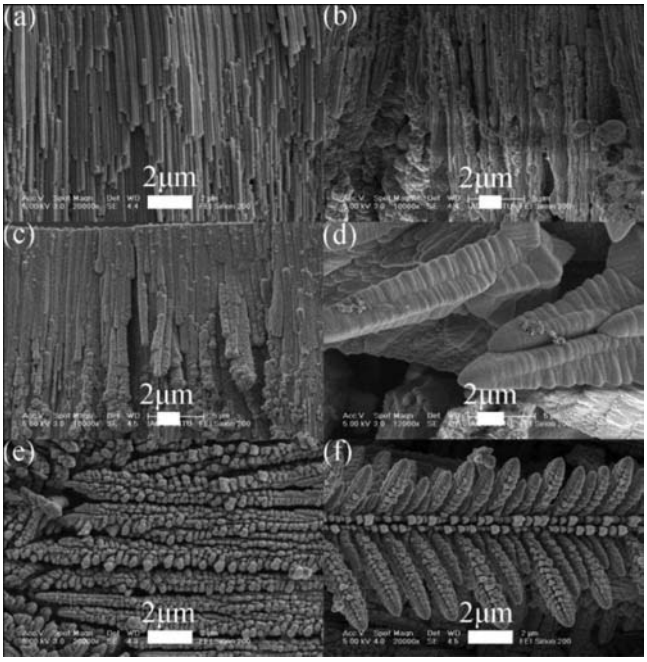

Figure 4. Typical SEM images of 3D STOMSs synthesized at different growth stages: (a) small amount of dissolution of TiNTs after 5 h, (b) large amount of dissolution of TiNTs and spontaneous nucleation at the cross section after 10 h, (c) oriented attachment within 10 × 2 h, (d) shaping of the 3D skeletons within 10 × 3 h, (e) formation of rods *via* chemical dissolution−precipitation within 10 × 4 h, (f) growth of rods within 10 × 5 h.

In conclusion, the synthesis of STOMSs undergoes several different stages, which are dissolution of TiNTs, spontaneous nucleation at the cross section, oriented attachment, shaping of the 3D skeleton, formation of rods *via* chemical dissolution−precipitation, and finally growth of the rods. Taking a panoramic view of all steps, there is another explanation for steps 0−4, which are similar to the synthesis of ZnO nanosheets, involving a 1D branching and subsequent 2D interspace filling theory.[43] But the difference is that the synthesis of $SrTiO_3$ undergoes a 3D interspace branching process. Then the filled skeleton dissolves and $SrTiO_3$ rods form and grow.

As an important part of the study on the synthesis mechanism, examining reaction products in the same reaction batch at different stages should be considered. X-ray diffraction patterns of the products show the presence of crystalline $SrTiO_3$ along with anatase TiO_2, as shown in Figure 5. It is obvious that the base lines show a slow increase between 0° and 37°, owing to the presence of anatase TiO_2. But as the reaction time goes on, the peaks of anatase TiO_2 disappear gradually after 10 × 5 h, which means a total transformation from anatase

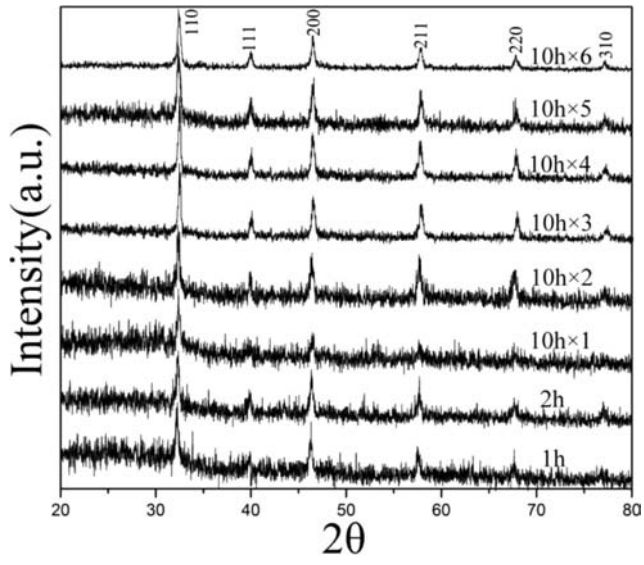

Figure 5. XRD patterns of the $SrTiO_3$ (perovskite) products obtained at different reaction times.

TiO_2 to crystalline $SrTiO_3$. Meanwhile, the gradually increase of peaks at 32.4°, 39.9°, 46.4°, 57.8°, 67.8°, and 77.2° can be indexed to (110), (111), (200), (211), (220), and (310) planes of $SrTiO_3$, suggesting the gradual formation of crystalline $SrTiO_3$. The SAED spectra of the STOMSs indicate that particles on the rods and skeletons are $SrTiO_3$ single crystals (Figure S3a and b). Meanwhile, EDS spectra of the samples show that the atomic percentage of Sr and Ti equals 1:1 (Figure S3c), which also means a total transformation from TiNTs to $SrTiO_3$. In conclusion, the precursor TiNTs show a good chemical reactivity as self-sacrifice templates to fabricate pure $SrTiO_3$ superstructures by adjusting the concentration of the mother liquors.

However, CO_2 in air would dissolve into our mother liquors and transform to CO_3^{2-} unavoidably, according to the equation below:

$$CO_2 + 2OH^- \rightarrow CO_3^{2-} + H_2O \quad (5)$$

The existence of CO_3^{2-} and Sr^{2+} would transform to $SrCO_3$ coated on $SrTiO_3$ superstructures and prevent nucleation of $SrTiO_3$. Even more, the target products will not be pure crystalline $SrTiO_3$ anymore. The precipitation of $SrCO_3$ takes place according to the following reaction:

$$Sr^{2+} + CO_3^{2-} \rightarrow SrCO_3 \quad (6)$$

To avoid this, excess $SrCl_2$ is added into the initial solutions to react with CO_3^{2-} to form $SrCO_3$ at first and CO_3^{2-} is depleted in the mother liquors. The precipitates of $SrCO_3$ need to be filtered to get clear mother liquors. XRD patterns of the precipitates (Figure S4) indicate that CO_3^{2-} has been transformed into $SrCO_3$ and been removed. For the further study of $SrTiO_3$ synthesized without additional control of KOH, SEM images of STO fabricated in different concentrations of OH^- without Ca^{2+} have been observed, as shown in Figure S5. It is clear that 3D STOMSs cannot be formed without additional control of KOH by Ca^{2+} in the hydrothermal reaction. As the solubility of $Sr(OH)_2$ is very low, Sr^{2+} reacts easily with OH^- to form a $Sr(OH)_2$ precipitate in hot mother liquors, and it is noticed that the solubility of $Ca(OH)_2$ is even lower than that of $Sr(OH)_2$. For instance, the solubility

dx.doi.org/10.1021/ic302585g | Inorg. Chem. 2013, 52, 2581−2587

of $Ca(OH)_2$ is 0.019 at 100 °C, while that of $Sr(OH)_2$ is 24.2. Hence, a small quantity of $CaCl_2$ is added to mother liquors and dissolves completely. OH^- will first precipitate the additional Ca^{2+} instead of Sr^{2+} at the surface of TiNTs, and Sr^{2+} reacts with $[Ti(OH)_6]^{2-}$ to form $SrTiO_3$. It is worth mentioning that $Ca(OH)_2$ will appear in the form of leaf-like structures coated on the STOMSs after the hydrothermal reaction, as shown in Figure S5d. Pure STOMSs are obtained by washing in a 1% dilute hydrochloric acid bath at 60 °C for 5 h to dissolve the fluffy $Ca(OH)_2$ layers and drying the as-obtained $SrTiO_3$.

Comparing with the multiple (five times) crystallization process, we carried out another batch experiment, which lasted about 5 days, with only one cooling crystallization process. Unfortunately, the 3D superstructures are not as perfect as that synthesized *via* multiple crystallization processes, as shown in Figure 6. What we could see are only the rudiments of

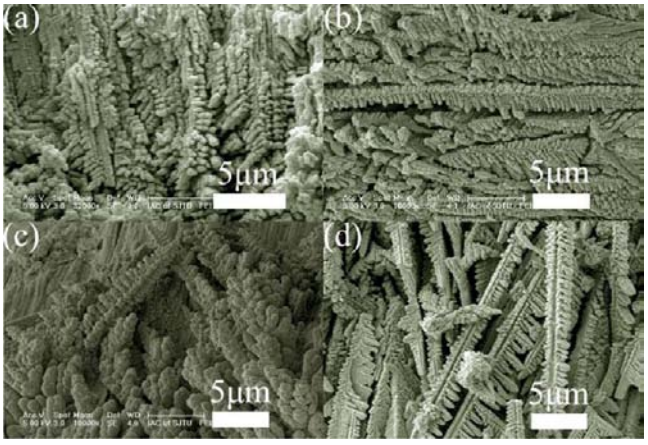

Figure 6. FESEM images of unshaped $SrTiO_3$ superstructures fabricated *via* one crystallization for 5 days in different mother liquors with variable concentrations of OH^-: (a) 0.5 M, (b) 1.0 M, (c) 1.5 M, (d) 2.0 M.

skeletons, which are not completely shaped, and the arrangement of $SrTiO_3$ rods on these skeletons is random and irregular. Hence, the importance of the method on multiple crystallization processes with rhythmic cooling is obvious, and this method is thought to be one of the easiest and most cost-effective in synthesizing high-quality 3D STOMSs.

More interestingly, these 3D STOMSs are demonstrated to have remarkable photoresponsive properties and considered to be a good photonic crystal. Thin films with periodic 3D structures show different colors from yellow to cyan, which are obvious by the naked eye. The controllability of these various colors can be realized by adjusting the pH value of the mother liquor, as shown in Figure S1b–d. Optical images and reflection spectra of colorful films were recorded by an optical microscope system with a CCD camera and spectrometer connected, as shown in Figure 7. The samples show a macroscopic average effect of diffraction colors by the naked eye, while varied colors could be observed in the optical microscope system, which indicated actual diffraction and interference effects of photons interacting with elementary micro- and nanostructures. Compared to general monochrome $SrTiO_3$ films, these 3D structured films respond in the visible region and show various reflected light from red to violet, which were characterized by several corresponding discrete peaks in the spectra. Addition-

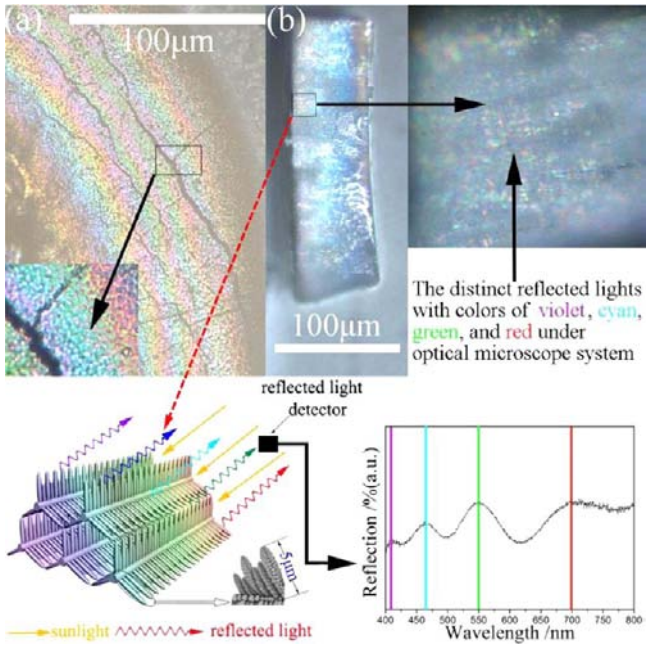

Figure 7. Optical reflections of a $SrTiO_3$ thin film with a thickness of about 100 μm, and the distinct reflected light with colors of violet, cyan, green, and red, respectively: (a) surface image and (b) cross section.

ally, the size (length and diameter) of the branches on the 3D superstructures can be controlled *via* reaction time and period, which means that the voids of the superstructures could also be adjusted simultaneously. These periodical and variable voids lead to refractive index modulations in three dimensions, adding more freedom to control the final morphology, which can lead to different photonic effects. Figure 7 shows the typical optical reflection spectra of the colorful films. The distinct reflection peaks located at 412, 465, 550, and 700 nm can be seen, corresponding to violet, cyan, green, and red, respectively.

For further confirmation that variable colors actually originate from diffraction and interference effects of photons interacting with elementary micro- and nanostructures, we obtained the reflectivity curves of STOMSs synthesized at different growth stages, as shown in Figure 8. The locations of reflection peaks vary from short wave to long wave (a to c), and after 10 × 4 h (d), more reflection peaks appear, which means different colors can be observed. It is clear that the colors at each growth stage are different, and the more complex the structures, the more colors that can be observed. Compared with these complex 3D structures, we also gathered the reflectivity curves of industrial STO powder (200 mesh) and single-crystal STO film (111), as shown in Figure S6. For the general monochrome $SrTiO_3$ film and powder, the reflectivity curve is nearly straight, which means that there is no photonic crystal effect.

Additionally, the colors of STOMSs can also be tuned by pH values. In the 1.0 M KOH system, the STO structures are mainly rods (rudiments) and are undiversified; the grating-analogous structures have not formed. In this case, only cyan can be observed based on photonic crystal theory (a certain structure possesses only a single color), while in 1.5 M or more KOH systems, grating-analogous structures, more colors will be reflected. It is difficult to distinguish each color by the naked eye in this situation, and what we can see is the macroscopic

dx.doi.org/10.1021/ic302585g | *Inorg. Chem.* 2013, 52, 2581–2587

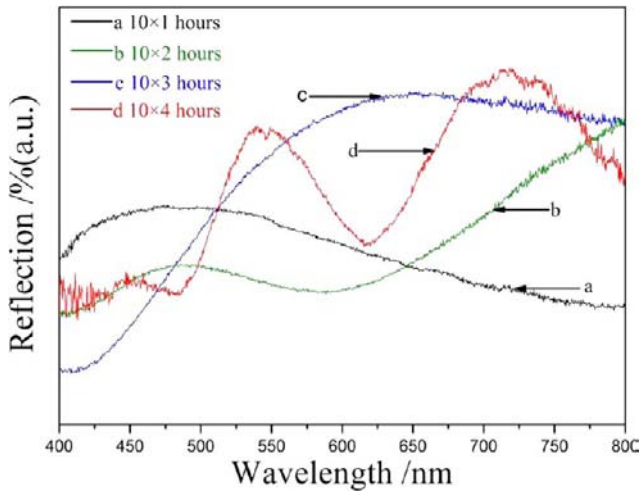

Figure 8. Reflectivity of STOMSs synthesized at different growth stages.

average effect (bright yellow) of diffraction colors. These varied colors could be observed in an optical microscope system, which indicated diffraction and interference effects of photons interacting with elementary micro- and nanostructures.

To get a further explanation for these different photonic effects, the theory of diffraction grating can be simply considered. It is obvious that branches and slits on the trunks constitute grating-analogous structures. If we simplify the complicated 3D interconnected microstructures of trunks and branches, only taking into account one side of the trunk, grating-analogous structures clearly exist (Figure 1d). Substituting the incident angle for 0 degrees, the grating equation can be simplified as below:

$$d \sin \theta = k\lambda \tag{7}$$

where d is the grating spacing, λ is the wavelength of incident light, and k is the order of the maximum. The values of the diffraction angle (θ) are generated by evaluating eq 7 for each λ, while the values of λ run in the visible region. It was calculated that the first-order rainbow of diffraction grating is generated from 15.83° to 27.67°, while maximal d_1 = 1.51 μm. Since the branches with different sizes are arranged alternately, there also exists a minimal d_2 = 1.12 μm, and the first-order rainbow of diffraction grating may be generated from 21.58° to 38.68°. These angles fall well in the collecting range of the microscope objective (N.A.= 0.75), but actually because the value of d varies from 1.12 to 1.51 μm, the final strong light diffraction effects lead to colored spots instead of rainbows, as shown in Figure 7b. However, if the distances of branches are constant, a single color will be displayed, which could be an indirect characterization of the order of the interbranch arrangement. Furthermore, these 2D well-ordered trunks along with branches of grating-analogous structures constitute 3D hybrid microstructures and contribute as well to light diffraction. The complexity of the superstructures and diffraction law of grating leads to the same phenomenon. Even though the incident angle is justified in the allowable range, the last result is only the position changes of spots, not the changes of colors, as shown in Figure 7b. In a word, diffraction and interference effects of photons based on the dimensions of the superstructures result in these four different colors. Since variable colors originate actually from modulation of the refractive indices of the superstructures, films with tunable colors can be obtained by adjusting the voids (grating spacing and gaps in the trunks) of the superstructures, and these are easily realized by varying the chemical reaction parameters. Hence new photoresponsive $SrTiO_3$ functional devices can be achieved in the future.

4. CONCLUSIONS

Self-assembled three-dimensional $SrTiO_3$ microscale superstructures have been prepared *via* hydrothermal synthesis and multiple (five times) crystallization processes, and this process is thought to be the key procedure of our synthesis. The length of each trunk on the microstructures is about 100 μm or more. What is more interesting, each branch on the trunk shows a corn-like structure. Periodical structures and diffraction grating effects lead to colorful photonic effects, and the colors are obvious, controllable, and vary from yellow to cyan to the naked eye. The distinct reflection peaks over the entire visible spectrum reveal the four colors violet, cyan, green, and red, respectively. This approach is simple and cost-effective in fabricating 3D STOMSs for practical photonic applications.

■ ASSOCIATED CONTENT

Ⓢ Supporting Information

Photo images of anodic TiO_2 at 90 V and hydrothermal-synthesized $SrTiO_3$ membranes, concentration variation of Sr, Ca, and Ti in mother liquors after hydrothermal reactions at different stages, TEM images and EDS spectra of STOMSs, and XRD patterns of the $SrCO_3$ precipitates. This material is available free of charge *via* the Internet at http://pubs.acs.org.

■ AUTHOR INFORMATION

Corresponding Author

*E-mail: mjzheng@sjtu.edu.cn. Tel: +86-021-34202791.

Author Contributions

All authors have given approval to the final version of the manuscript.

Notes

The authors declare no competing financial interest.

■ ACKNOWLEDGMENTS

This work was supported by the Natural Science Foundation of China (Grant Nos. 11174197, 91123006), National Major Basic Research Project of China (Grant Nos. 2012CB934302, 2012CB932303), and National 863 Program 2011AA050518.

■ REFERENCES

(1) Chandler, C. D.; Roger, C.; Hampden-Smith, M. J. *Chem. Rev.* **1993**, *93*, 1205−1241.
(2) Kim, Y.; Woodward, P. M.; Baba-Kishi, K. Z.; Tai, C. W. *Chem. Mater.* **2004**, *16*, 1267−1276.
(3) Pena, M. A.; Fierro, J. L. G. *Chem. Rev.* **2001**, *101*, 1981−2017.
(4) Scott, J. F. *Science* **2007**, *315*, 954−959.
(5) Bhalla, A. S.; Guo, R.; Roy, R. *Mat. Res. Innovations* **2000**, *4*, 3−26.
(6) Scott, J. F.; Morrison, F. D. *Ferroelectrics* **2008**, *371*, 3−9.
(7) Tabata, H.; Kawai, T. *Appl. Phys. Lett.* **1994**, *65*, 1970−1972.
(8) Mi, Y. Y.; Yu, Z.; Wang, S. J.; Gao, X. Y.; Wee, A. T. S.; Ong, C. K.; Huan, C. H. A. *J. Appl. Phys.* **2007**, *101*, 063708.
(9) Kato, H.; Kudo, A. *J. Phys. Chem. B* **2002**, *106*, 5029−5034.
(10) Cardona, M. *Phys. Rev.* **1965**, *140*, 651−655.
(11) Li, Y.; Gao, X. P.; Li, G. R.; Pan, G. L.; Yan, T. Y.; Zhu, H. Y. *J. Phys. Chem. C* **2009**, *113*, 4386−4394.
(12) Wold, A.; Dwight, K. *J. Solid State Chem.* **1990**, *88*, 229−238.
(13) Merkle, R.; Maier, J. *Angew. Chem., Int. Ed.* **2008**, *47*, 3874−3894.

(14) Wills, L. A.; Wessels, B. W.; Richeson, D. S.; Marks, T. J. *Appl. Phys. Lett.* **1992**, *60*, 41−43.
(15) Zhao, J.; Fuflyigin, V.; Wang, F.; Norris, P. E.; Bouthilette, L.; Woods, C. *J. Mater. Chem.* **1997**, *7*, 933−936.
(16) Nam, S. H.; Lee, W. J.; Kim, H. G. *J. Phys. D: Appl. Phys.* **1994**, *27*, 866−870.
(17) Mackenzie, J. D.; Xu, Y. H. *J. Sol−Gel Sci. Technol.* **1997**, *8*, 673−679.
(18) Kamalasanan, M. N.; Kumar, N. D.; Chandra, S. *J. Appl. Phys.* **1993**, *74*, 679−686.
(19) Wu, Z.; Kumagai, N.; Yoshimura, M. *Chem. Mater.* **2000**, *12*, 3356−3361.
(20) Zhang, S.; Liu, J.; Han, Y.; Chen, B.; Li, X. *Mater. Sci. Eng., B* **2004**, *110*, 11−17.
(21) Jing, Y.; Jin, S.; Jia, Y. Z.; Han, J. D.; Sun, J. H. *J. Mater. Sci.* **2005**, *40*, 6315−6317.
(22) Wang, Y.; Xu, H.; Wang, X.; Zhang, X.; Jia, H.; Zhang, L.; Qiu, J. *J. Phys. Chem. B* **2006**, *110*, 13835−13840.
(23) Dong, W.; Li, B.; Li, Y.; Wang, X.; An, L.; Li, C.; Chen, B.; Wang, G.; Shi, Z. *J. Phys. Chem. C* **2011**, *115*, 3918−3925.
(24) Yu, S. H.; Cölfen, H.; Tauer, K.; Antonietti, M. *Nat. Mater.* **2005**, *4*, 51−55.
(25) Gu, Z.; Zhai, T.; Gao, B.; Zhang, G.; Ke, D.; Ma, Y.; Yao, J. *Cryst. Growth Des.* **2007**, *7*, 825−830.
(26) Zhu, L. P.; Xiao, H. M.; Zhang, W. D.; Yang, Y.; Fu, S. Y. *Cryst. Growth Des.* **2008**, *8*, 1113−1118.
(27) Zhu, T. J.; Chen, X.; Cao, Y. Q.; Zhao, X. B. *J. Phys. Chem. C* **2009**, *113*, 8085−8091.
(28) Querejeta-Fernández, A.; Hernández-Garrido, J. C.; Yang, H.; Zhou, Y.; Varela, A.; Parras, M.; Calvino-Gámez, J. J.; González-Calbet, J. M.; Green, P. F.; Kotov, N. A. *ACS Nano* **2012**, *6*, 3800−3812.
(29) Engelkamp, H.; Middelbeek, S.; Nolte, R. J. M. *Science* **1999**, *284*, 785−788.
(30) Fei, J.; Cui, Y.; Yan, X.; Yang, Y.; Su, Y.; Li, J. *J. Mater. Chem.* **2009**, *19*, 3263−3267.
(31) Zhao, C. P.; Zhang, X. W.; Zhang, Y. P.; Xing, Y. L.; Zhang, X. J.; Zhang, X. H.; Jie, J. S. *CrystEngComm* **2012**, *14*, 819−823.
(32) Mishina, E.; Zaitsev, A.; Ilyin, N.; Sherstyuk, N.; Sigov, A.; Golovko, Y.; Muhortov, V.; Kolesnikov, A.; Lozovik, Y.; Yemtsova, M.; Rasing, T. *Appl. Phys. Lett.* **2007**, *91*, 041107.
(33) Lin, P. T.; Liu, Z.; Wessels, B. W. *J. Opt. A: Pure Appl. Opt.* **2009**, *11*, 075005.
(34) Yuan, X. L.; Zheng, M. J.; Ma, L.; Shen, W. Z. *Nanotechnology* **2010**, *21*, 405302.
(35) Calderone, V. R.; Testino, A.; Buscaglia, M. T.; Bassoli, M.; Bottino, C.; Viviani, M.; Buscaglia, V.; Nanni, P. *Chem. Mater.* **2006**, *18*, 1627−1633.
(36) Wei, X.; Vasiliev, A. L.; Padture, N. P. *J. Mater. Res.* **2005**, *20*, 2140−2147.
(37) Eckert, J. O.; Hung-Houston, C. C.; Gersten, B. L.; Lencka, M. M.; Riman, R. E. *J. Am. Ceram. Soc.* **1996**, *79*, 2929−2939.
(38) Zheng, M. J.; Zhang, L. D.; Li, G. H.; Shen, W. Z. *Chem. Phys. Lett.* **2002**, *363*, 123−128.
(39) Chen, B.; Xu, Q.; Zhao, X.; Zhu, X.; Kong, M.; Meng, G. *Adv. Funct. Mater.* **2010**, *20*, 3791−3796.
(40) Lee, E. J. H.; Ribeiro, C.; Longo, E.; Leite, E. R. *J. Phys. Chem. B* **2005**, *109*, 20842−20846.
(41) Zhang, Q.; Liu, S. J.; Yu, S. H. *J. Mater. Chem.* **2009**, *19*, 191−207.
(42) Testino, A.; Buscaglia, M. T.; Buscaglia, V.; Viviani, M.; Bottino, C.; Nanni, P. *Chem. Mater.* **2004**, *16*, 1536−1543.
(43) Park, J. H.; Choi, H. J.; Choi, Y. J.; Sohn, S. H.; Park, J. G. *J. Mater. Chem.* **2004**, *14*, 35−36.